Engineering Solid Mechanics 14 (2026) 273-282

Contents lists available at GrowingScience

Engineering Solid Mechanics

homepage: www.GrowingScience.com/esm

Investigation of strength material for additive manufacturing using 3d metal printer

M. B. Ali[a*], Ahmad Nazirul Mubin Bin Nezam[b], H. Zainuddin[c], S. A. Ismail[a] and Lailatul Harina Paijan[a]

[a]*Faculty of Industrial and Manufacturing Engineering Technology, Universiti Teknikal Malaysia Melaka, Hang Tuah Jaya, 76100 Durian Tunggal, Melaka, Malaysia*
[b]*Yeong Chaur Shing Paper Mill Sdn. Bhd., Lot 736, Mukim Tampoi Krubong, 75250 Melaka Tengah, Melaka, Malaysia*
[c]*Faculty of Mechanical and Engineering Technology, Universiti Teknikal, Malaysia Melaka, Hang Tuah Jaya, 76100 Durian Tunggal, Melaka, Malaysia*

ARTICLE INFO

Article history:
Received 12 January 2026
Accepted 15 April 2026
Available online
15 April 2026

Keywords:
Stainless steel 316L
Aluminium 6061-T6
Charpy impact
Impact duration
Impact energy absorbed
Stainless steel 304
Strain signal

ABSTRACT

Rapid advances in 3D printing enable the automotive sector to shorten the design cycles, improve flexibility and support customised manufacturing, overcoming the limitations of conventional methods. However, direct comparisons of impact performance particularly those employing instrumented techniques to analyse strain–time signals between SLM-produced SS 316L specimens of varying thicknesses and these specific conventional reference materials remain limited, leading to uncertainty regarding the use of Additive Manufacturing (AM) parts in safety-critical applications. This study aims to assess the strength of additive manufacturing Stainless Steel 316L (SS 316L) powder at various specimen thicknesses and to compare it against the conventional SS 304 and Al 6061-T6. To capture the strain signal, a Charpy machine, a data acquisition system and strain gauges were used in the experiment. Specimen preparation followed the ASTM E8 for tensile test and ASTM E23 for the Charpy impact. Charpy specimens with thicknesses 5, 7.5 and 10 mm were fabricated using an Ermaksan Enavision 120 Selective Laser Melting (SLM) 3D printer under controlled parameters. Results show that increase in specimen thicknesses proportionally increase the absorbed energy and the area under the curve. Compared to reference material, SS 304 exhibited highest impact resistance, followed by AM SS 316L and Al 6061-T6. These findings demonstrate that AM materials can closely match the performance of conventional material. Furthermore, optimising SLM parameters and applying post-processing can improve impact toughness.

© 2026 Growing Science Ltd. All rights reserved.

1. Introduction

Additive manufacturing (AM) of SS 316L has emerged as a transformative technology, enabling the fabrication of complex geometries with tailored mechanical properties for critical applications in aerospace, medical, and energy sectors. The mechanical reliability of AM-fabricated SS 316L, particularly under tensile and impact loading, is a central concern for its widespread adoption. Recent research has focused on understanding and optimizing the tensile and impact properties of SS 316L produced by various AM techniques, such as wire arc additive manufacturing (WAAM), laser powder bed fusion (L-PBF), and sinter-based extrusion. Theoretically, the Charpy impact energy absorbed by a specimen is determined from the difference between the pendulum's height of fall and its height of rise. A greater height of rise indicates a higher amount of energy absorbed.

$$U = mg(h - h^{1}) \tag{1}$$

$$U = mgS(\cos\beta - \cos\alpha) \tag{2}$$

where U represents the absorbed energy, m is the mass of the pendulum, g denotes gravitational acceleration, h is the initial height of the striker, h' is the height of rise, S is the length of the pendulum to the striker's centre, β is the angle of fall, and α is the angle of rise. WAAM has demonstrated the ability to produce multi-layered SS 316L structures with mechanical properties, including tensile and impact strength, comparable to or exceeding those of wrought materials. Microstructural analysis reveals well-bonded layers, minimal defects, and a combination of columnar and dendritic grains, contributing to consistent microhardness and superior impact strength (Vora et al., 2022). However, studies on L-PBF have highlighted

* Corresponding author.
E-mail addresses: basri@utem.edu.my (M.B. Ali)

ISSN 2291-8752 (Online) - ISSN 2291-8744 (Print)
© 2026 Growing Science Ltd. All rights reserved.
doi: 10.5267/j.esm.2026.4.004

significant variability in tensile performance across different machines, even when using identical parameters and powder batches, underscoring the influence of machine-specific factors on mechanical outcomes (Obeidi et al., 2021).

The microstructural evolution during AM, including grain size, phase distribution, and porosity, plays a pivotal role in determining mechanical behaviour. Sinter-based extrusion methods have produced near-fully dense SS 316L with mechanical properties meeting industrial standards, though the presence of microporosity and inclusions can affect fracture modes (Santamaría et al., 2022). The printing-debinding-sintering (PDS) pathway has also been shown to yield components with satisfactory tensile and fatigue properties, though pore-induced voids can impact crack propagation (Jiang & Ning, 2021). Post-processing treatments and environmental factors further influence mechanical performance. Neutron irradiation and heat treatments can lead to hardening and reduced ductility, with the extent of property changes depending on the initial microstructure and treatment conditions (Konstantinović et al., 2025). In situ neutron diffraction and high-energy X-ray studies have provided insights into anisotropy, deformation mechanisms, and the role of microstructural features in tensile and impact behaviour (Chen et al., 2025; Zhang et al., 2020).

Build orientation, specimen thickness, and process parameters are critical in optimizing mechanical properties. Studies have shown that certain build orientations and minimum thicknesses are necessary to achieve mechanical properties equivalent to conventionally manufactured SS 316L (Carassus et al., 2022; Coughlin et al., 2020). Advanced WAAM methods, such as pulsed arc plasma and cold metal transfer, have enabled simultaneous improvements in strength, ductility, and impact toughness (Duan & Yang, 2023; Lone et al., 2024; Kumar et al., 2024).

Comparative studies between AM techniques, such as L-PBF and binder jetting, reveal that L-PBF generally produces finer grain structures and higher tensile strength, while binder jetting may result in lower density and mechanical performance (Xu et al., 2023). The development of bi-metallic structures and multi-material builds further expands the potential of AM for engineering applications requiring exceptional mechanical properties (Subramaniyan & Thirugnanasambandam, 2024).

This study adopts an experimental approach consistent with earlier work, in which strain gauges were mounted at the point of impact and the resulting strain signals recorded to determine the absorbed energy (Shterenlikht et al., 2005; Ali et al., 2015; Muhammad Said et al., 2018). Previous research reported tests on various materials using the instrumented Charpy impact method specifically stainless steel 304, aluminium alloy 6061-T6, and aluminium alloy 7075-T6, providing valuable insight into the impact response of each material under instrumented testing (Zainuddin et al., 2024).

This study investigates stainless steel 316L specimens of varying thickness produced by additive manufacturing, alongside tests on Stainless Steel 304 and Aluminium Alloy 6061-T6, using the instrumented Charpy impact method. During testing, the Charpy machine records the absorbed energy while the impact strain signal is captured simultaneously. These results are crucial for assessing the impact response of each material, particularly additively manufactured SS 316L and for revealing the distinct signal patterns of each, which reflect both impact duration and the area beneath the curve.

2. Methodology

2.1 Material Preparation

The specimens for the Charpy impact test were prepared using the SLM process with the Ermaksan Enavision 120 SLM 3D metal printer. Specimen drawings with dimensions in accordance with ASTM E23 and ASTM E8 standards were created using CAD software. These CAD files were then converted into STL format to enable the 3D printer to fabricate the required specimens. Once the STL files were imported into the printer software, the printing process commenced, building the specimens layer by layer. The Charpy specimen conformed to the standard dimensions: 55 mm in length and 10 mm in both height and width. They were of the V-notch type, featuring a 45° notch angle, a root radius of 0.25 mm, and a notch depth of 2 mm. For the tensile test, three specimens of SS 316L were prepared in accordance with ASTM E8.

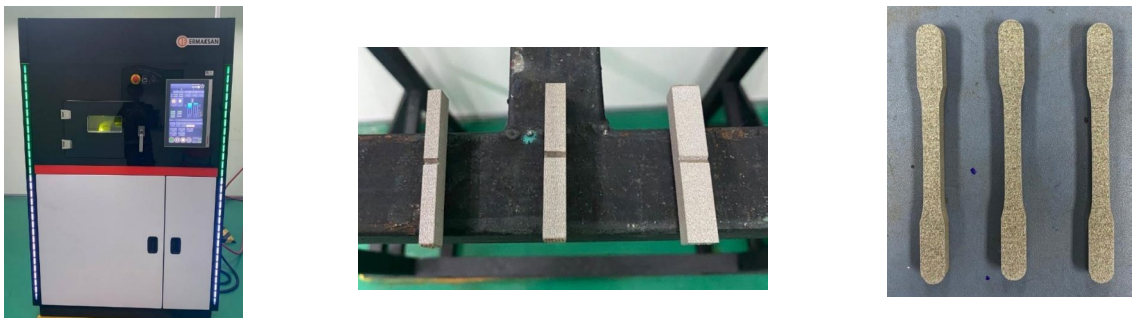

(a) (b) (c)

Fig. 1. (a) Ermaksan Enavision 120 SLM 3D Printer metal, (b) charpy impact specimen and (c) tensile specimen for Stainless Steel 316 L.

Fig. 1 illustrates the Ermaksan Enavision 120 SLM 3D metal printer, the Charpy impact specimen, and the tensile specimen. The selected process parameters included a voltage of 230 V, a laser scanning speed of 900–1000 mm/s, a current of 32 A, laser power ranging from 130 to 240 W, a layer thickness of 0.04 mm, a hatch spacing of 0.1 mm, a laser diameter 0.075 mm, the use of argon and nitrogen as inert gases, and an oxygen level of 2500 ppm. For comparison, conventional materials, SS 304 and Al 6061-T6, were prepared in accordance with ASTM E23 standard for the Charpy impact test to ensure consistency with the 3D printed SS 316L specimens. These two reference materials were selected due to their widespread use in structural applications such as architecture, construction, automotive, and aerospace industries. The material properties are summarised in **Table 1**.

Table 1. Material properties (Beer et al., 2020; Shackelford, 2015)

Material properties	Material		
	Stainless Steel 316L	Stainless Steel 304	Aluminium 6061-T6
Tensile Strength (MPa)	582.07	603.81	314.40
Yield Strength (MPa)	310.10	306.35	260.57
Young's Modulus (GPa)	193	193	70
Density (kg/m^3)	7900	7800	2710

2.2 Experimental Work

In this study, Charpy impact testing was carried out on SS S316L specimens produced using the SLM 3D printing method with thicknesses of 10 mm, 7.5 mm, and 5 mm. Three samples were prepared for each thickness, and the results were compared accordingly. The SS 316L specimens with a thickness of 10 mm were then compared with conventionally manufactured SS 304 and Al 6061-T6. Several parameters were evaluated, namely the absorbed energy (experimental and theoretical), the area under the strain–time graph, impact duration, and maximum strain signal. The objective of this comparison was to assess the impact strength of materials produced by SLM 3D printing (SS 316L) against conventionally manufactured counterparts, namely Al 6061-T6 and SS 304.

2.3 Equipment and Instrumentation

The Charpy impact testing machine used in this experiment has a maximum capacity of 250 Joules and an impact speed of 5.24 m/s. The complete instrumented Charpy impact setup includes the apparatus and instruments illustrated in **Fig. 2**. Before conducting the test, a 2 mm KYOWA strain gauge was glued to the sides of the pendulum impactor, as shown in **Figure 2(c)**. The strain signals are collected using a SOMAT eDAQ Lite data acquisition system, connected to a laptop for real-time data display. Additionally, the Charpy machine is connected to a computer equipped with WinImpact software. This application records basic test data such as impact energy, angle of fall, and angle of rise, as shown in **Fig. 3**.

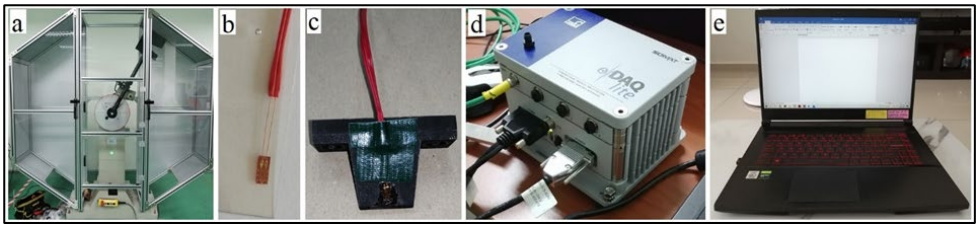

Fig. 2. Apparatus and instruments used in the Charpy test: (a) 250 J Charpy impact machine, (b) strain gauge, (c) strain gauge attached to the impactor, (d) data acquisition system (eDAQ), (e) computer for results display.

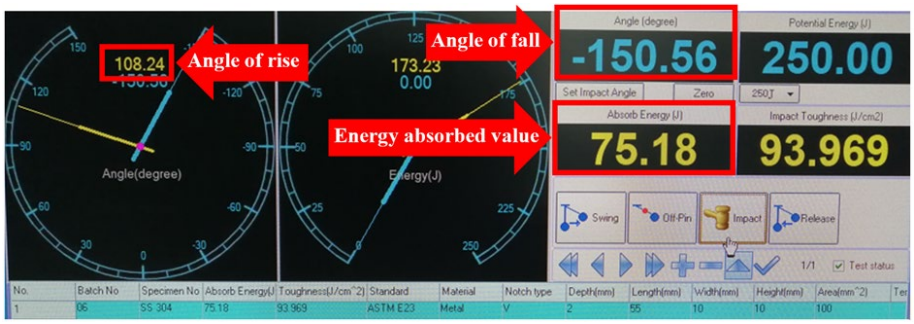

Fig. 3. Example output from WinImpact software, displaying key data including the angle of fall, angle of rise, and absorbed energy.

3. Results and Discussion

The impact strain signals for SS 316L specimens with thicknesses of 5 mm, 7.5 mm, and 10 mm are presented in **Fig. 4**, **Fig. 5,** and **Fig. 6**. For clearer comparison, the signals for the different thicknesses are combined, as illustrated in **Fig. 7**. All graphs have been optimised and analysed within the time range of 0 to 3.5 milliseconds. Deformation begins at approximately 0.5 milliseconds and ends before 2.5 milliseconds, which corresponds to the impact duration. When focusing on the strain deformation section of the graphs, each thickness displays a distinct curve pattern. The 10 mm specimen shows a larger area under the curve compared with the other two thicknesses. In contrast, the 7.5 mm specimen exhibits a curve that is broader and less sharp than that of the 5 mm specimen. These differences are further highlighted through analysis of the area under the curve derived from the obtained graphs.

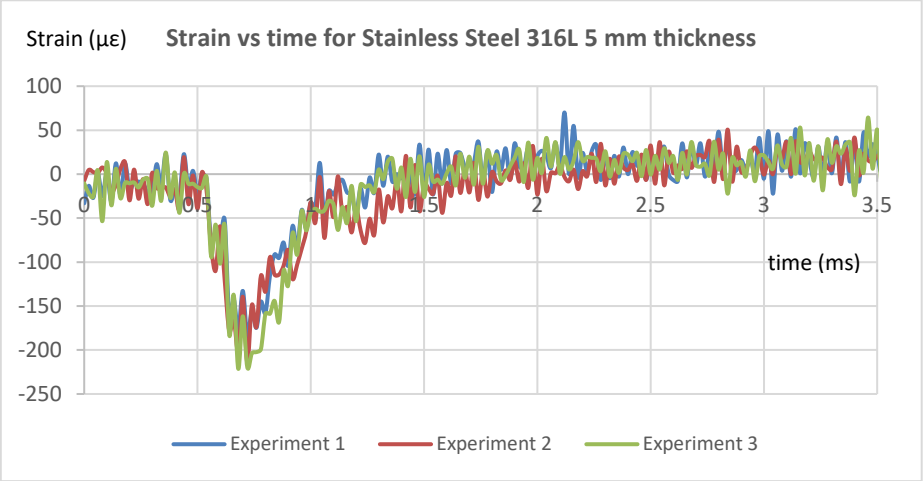

Fig. 4. Strain-time curve for SS 316L 5 mm thickness

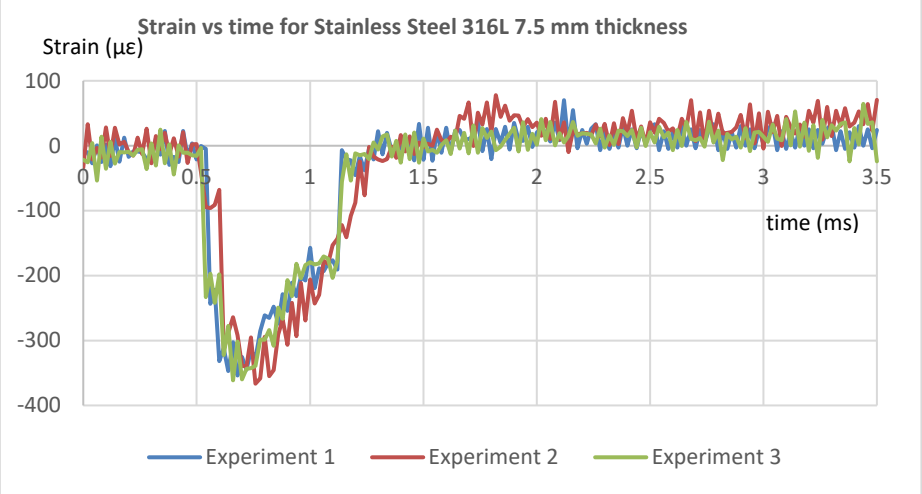

Fig. 5. Strain-time curve for SS 316L 7.5 mm thickness

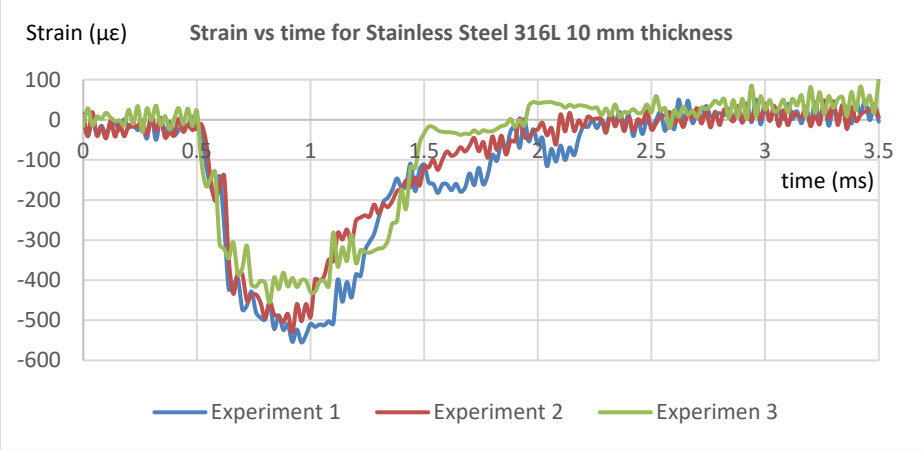

Fig. 6. Strain-time curve for SS 316L 10.0mm thickness

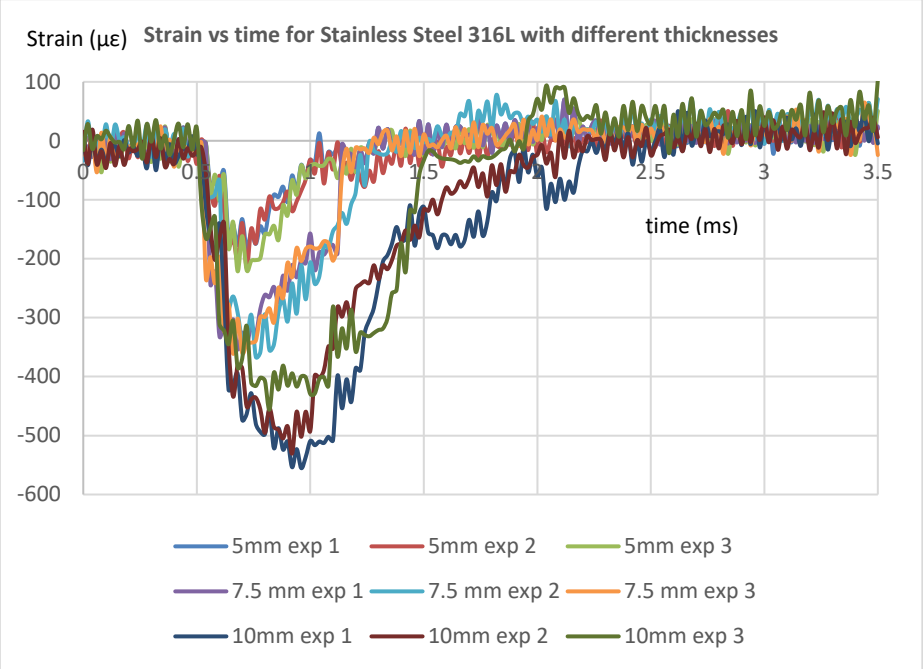

Fig. 7. Strain-time curve for SS 316L for different thicknesses

Table 2 and **Fig. 8** present the comparison between the area under the strain–time graph and the absorbed energy. The results indicate that the 10 mm specimen records both greater absorbed energy and a larger area under the curve compared with the 7.5 mm and 5 mm specimens. A clear proportional relationship is observed between the absorbed energy and the corresponding area under the curve. These findings agree with those reported by Muhammad Said et al. (2018), who demonstrated that as specimen thickness increases, both absorbed energy and the area under the strain-time curve increase in a directly proportional manner.

Table 2. Data of Charpy impact test (absorbed energy) and area under curve of SS 316 L for different thickness

		Thickness 5 mm	Thickness 7.5 mm	Thickness 10 mm
Experiment Energy Absorbed (J)	Exp 1	13.06	21.46	37.14
	Exp 2	14.88	20.96	49.72
	Exp 3	15.66	22.80	46.59
	Average	14.53 J	21.74 J	44.48 J
Area under Curve (με.ms)	Exp 1	54.82	154.36	308.05
	Exp 2	70.02	150.86	428.67
	Exp 3	73.66	161.15	348.79
	Average	66.16 με.ms	155.46 με.ms	361.83 με.ms

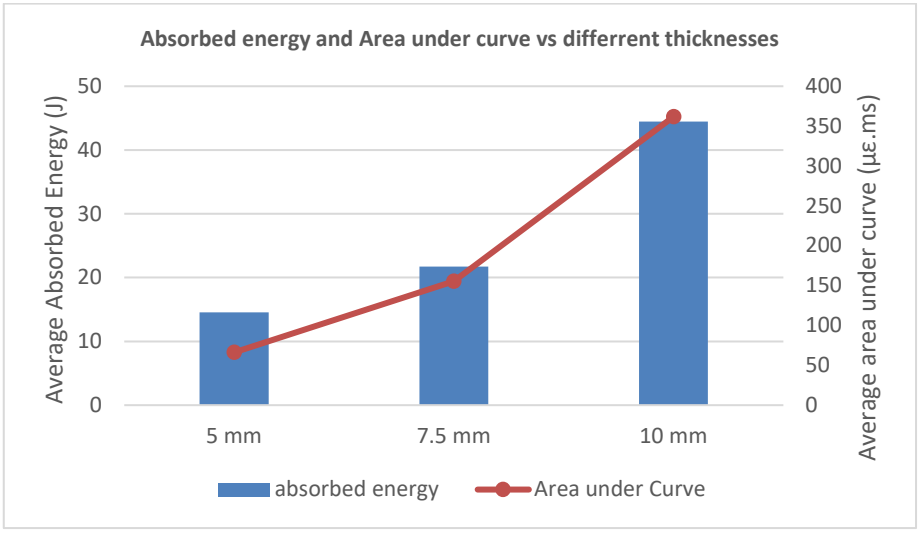

Fig. 8. Absorbed energy and area under curve for different thicknesses

Fig. 9 presents a comparison of the strain–time curves for different materials, namely Aluminium 6061-T6, Stainless Steel 304, and Stainless Steel 316L. Stainless Steel 304 exhibits a larger area under the curve and higher absorbed energy compared with the other two materials. Stainless Steel 316L, on the other hand, lies between Aluminium 6061-T6 and Stainless Steel 304. This pattern indicates that the impact strength of Stainless Steel 316L produced by 3D printing is moderate, falling between the two reference materials. Experimental evidence confirms that SS 304 has the highest impact strength and energy absorption, Al 6061-T6 the lowest, and SS 316L (or its composites) falls in between (Zainuddin et al., 2024; Zhang et al., 2022). The INL (Byun & Smidts, 2004) report compares 304L vs 316L and indicates that 304L exhibits a greater capacity to absorb impact energy than 316L.

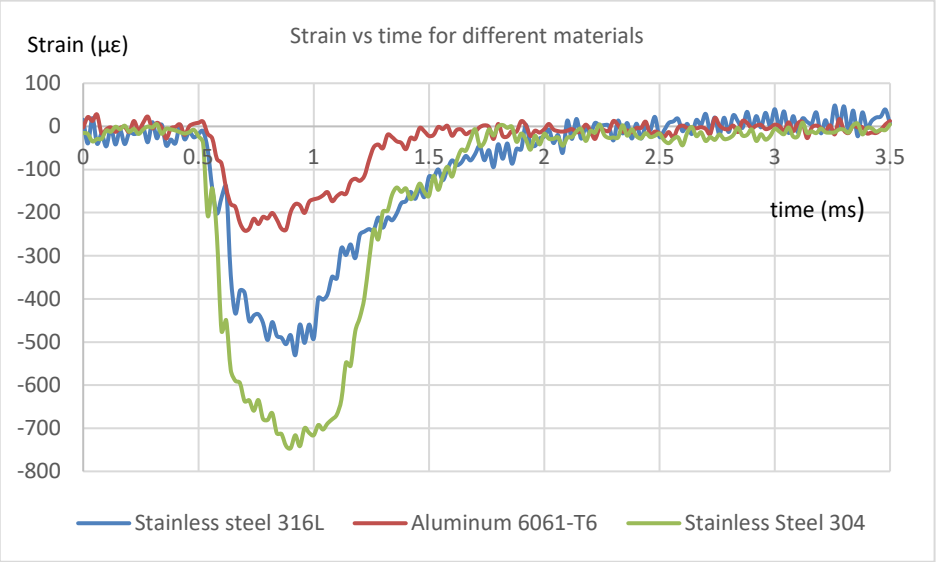

Fig. 9. Comparison of Strain–Time Curves for Different Materials

To improve the understanding of the strain–deformation curve, the discussion explores in greater depth the analysis of impact duration and maximum strain. Key parameters, including impact duration, maximum strain, and the area under the curve, were extracted from the graphs and are presented in **Table 3**. The experiments were conducted in triplicate, and the average values were calculated and reported in **Table 3.**

Table 3. Data for each material

		Stainless Steel 316L	Stainless Steel 304	Aluminium 6061-T6
Experiment Energy Absorbed (J)	Exp 1	37.14	90.00	13.75
	Exp 2	49.72	85.00	18.75
	Exp 3	46.59	76.50	15.00
	Average	44.48	83.83	15.83
Theory Energy Absorbed (J)	Exp 1	36.68	85.66	14.38
	Exp 2	47.73	82.05	17.47
	Exp 3	44.87	75.34	13.03
	Average	43.09	81.02	14.96
Maximum Strain (με)	Exp 1	555.21	746.06	250.57
	Exp 2	530.56	816.47	241.46
	Exp 3	456.16	795.20	247.35
	Average	513.98	785.91	246.46
Impact Duration (millisecond)	Exp 1	1.50	1.24	0.90
	Exp 2	1.42	1.32	1.24
	Exp 3	1.28	1.80	0.94
	Average	1.40	1.45	1.03
Area under Curve (με.ms)	Exp 1	308.05	473.78	89.47
	Exp 2	428.67	456.58	135.60
	Exp 3	348.79	484.010	76.93
	Average	361.83	471.49	100.67

An example application of Eq. (1) is shown here. By substituting the values from Eq. (2), where *mg* (pendulum weight) = 178.17 N, S = 0.748 m, β = 150.56°, and α = 108.24°.

$$U = (178.17)(0.748)(\cos 150.56 - \cos 108.24)$$

$$U = 74.32J$$

The comparison between experimental and theoretical absorbed energy values indicates that the experimental results are consistently higher. This variation is attributed to energy losses occurring during testing, mainly due to friction and windage (ASTM E23-18, n.d.).

Among the materials, SS 304 exhibits the highest absorbed energy in both experimental and theoretical results, followed by SS 316L and AA 6061-T6.

A 2024 study investigated the impact properties of SS 304, AA 6061-T6, and AA 7075-T6 using instrumented Charpy tests. The findings revealed that Stainless Steel 304 exhibited the highest energy absorption, longest impact duration, and greatest area under the curve, followed by Aluminium 6061-T6 and Aluminium 7075-T6 (Zainuddin et al., 2024). Although SS 316L is recognised for its favourable impact energy, the evidence confirms that stainless steels in general possess higher impact energy than many other alloys (Bunchoo et al., 2022).

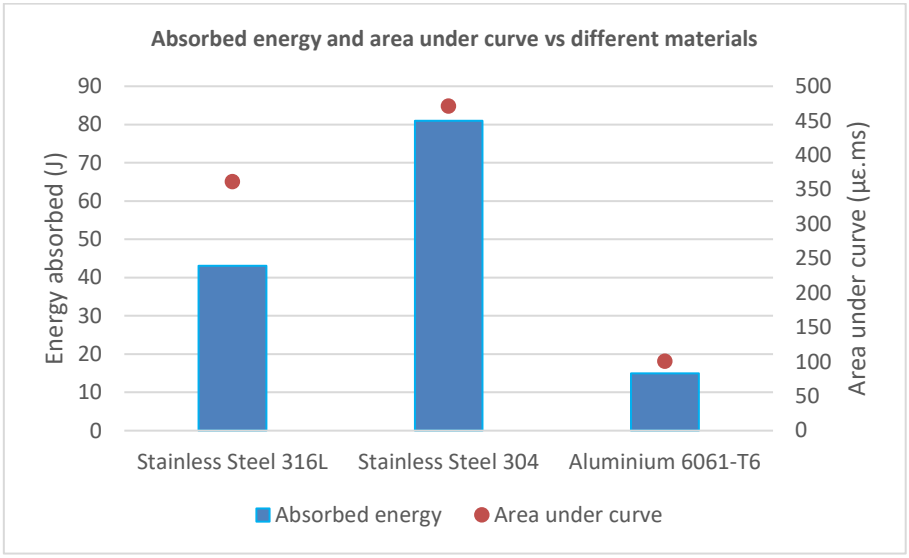

Fig. 10. Correlation of the energy absorbed and area under the curve

Fig. 10 depicts the relationship between absorbed impact energy and the area beneath the strain–time curve. The curve exhibits a trend analogous to that of the absorbed energy, with its area increasing in proportion to the energy absorbed (Muhammad Said et al., 2016; Zhang et al., 2022; Xia et al., 2022). In summary, SS 304 shows the greatest impact response, followed by stainless steel 316L and AA 6061-T6. When the impactor strikes the specimen, deformation occurs while the strain gauge simultaneously records the resulting impact strain. The specimen continues to deform and ultimately fractures within the defined impact duration. Materials possessing higher internal energy or a greater capacity for plastic deformation display superior impact-energy absorption (Li et al., 2023). Overall, the impact-strain signal serves as a dependable indicator of energy-absorption behaviour, as the area under the curve accurately reflects the absorption trend. This observation provides valuable insight into the link between absorbed energy and the pattern of the impact-strain signal.

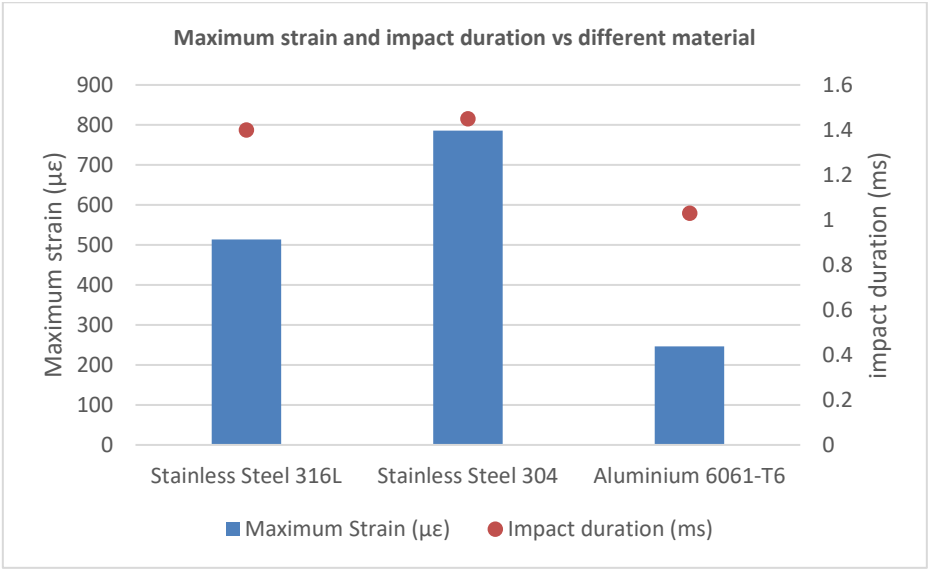

Fig. 11. Impact duration and maximum strain for the material experimented

Fig. 11 presents a comparison of impact duration and maximum strain for all the tested materials. No significant correlation is observed between impact duration and maximum strain. The impact duration is influenced by the rate of deformation and fracture of the material. Material deformation is proportional to strain; thus, greater deformation results in higher maximum strain. An increase in impact energy likewise leads to a higher maximum displacement value (Ivañez et al., 2015).

Notably, the maximum strain of SS 304 is approximately 52.9 % greater than that of SS 316L. Previous research reports that SS 304 and SS 316 differ in their deformation behaviour, particularly beyond the onset of necking, with SS 304 generally exhibiting higher strain in certain regions of the true stress–strain curve (Kweon et al., 2020). Radha and Sreekanth (2015) compare the yield strength, tensile strength and elongation of 304L and 316L, showing that 304L typically possesses higher elongation (and therefore greater strain capacity).

Although tensile and yield strengths are key mechanical properties, impact resistance also depends on ductility and percentage elongation, as these characteristics enable greater deformation before fracture. This difference is likely attributable to the distinct alloying-element compositions of the steels. Such assessments of material properties are essential when selecting materials for specific applications.

As shown in **Fig. 11**, SS 304 exhibits a noticeably longer impact duration than the other materials. This extended duration indicates that the steel undergoes a slower rate of deformation and fracture under impact loading. Such behaviour is significant, as it allows greater dissipation of kinetic energy during the impact event. SS 316L shows the next longest impact duration, while AA 6061-T6 records the shortest.

Chen et al. (2018) report that austenitic stainless steels (including 304) exhibit longer impact durations and lower strain-rate sensitivity than aluminium alloys, leading to improved energy dissipation during impact. Prashanth et al. (2019) report that SS 304 generally displays a longer time to fracture and higher absorbed energy than SS 316L and AA 6061-T6.

This suggests that the materials differ in their ability to withstand deformation, leading to variations in impact duration. In crashworthiness applications, a longer impact duration is advantageous because it provides more time for energy dissipation during a collision, thereby reducing the peak force at the end of the impact event (Chen et al., 2018; Prashanth et al., 2019; Lu & Yu, 2003).

Overall, SS 304 performs best across all impact properties, making it an excellent base material for energy-absorbing structural applications compared with the other two materials. When applications place greater emphasis on factors such as lightweight design, density, material cost, manufacturability, recyclability and life-cycle considerations, automotive fabrication typically requires the integration of multiple materials (Chen et al., 2018; Prashanth et al., 2019; Tisza & Czinege, 2018).

Although SS 304 offers outstanding impact resistance, a comparison with the 3D-printed material SS 316L shows that the latter also demonstrates good impact capability, falling between SS 304 and aluminium 6061-T6. The use of additive manufacturing for producing ferrous and steel components can continue to be improved so that, over time, the resulting materials can match the performance of those produced by conventional methods.

4. Conclusion

The investigation demonstrates a clear relationship between specimen thickness, absorbed energy, and the area under the strain–time curve for additively manufactured SS 316L. As thickness increased from 5 mm to 10 mm, both absorbed energy and the corresponding curve area rose proportionally, confirming the direct link between impact strain signals and energy absorption.

When compared with the reference materials, conventionally processed SS 304 consistently showed the highest impact resistance, followed by 3D-printed SS 316L and Al 6061-T6. SS 304 exhibits superior impact performance compared with aluminium, indicating that stainless steel is the most suitable material for use in impact-energy-absorbing devices. An effective energy absorber should withstand high levels of impact energy over a prolonged duration and accommodate substantial maximum strain. High internal energy and the ability to undergo plastic deformation contribute to excellent energy-absorption capacity.

Typical additive manufacturing (AM) microstructures in stainless steel, such as fine grains, melt pool boundaries, and defects like lack-of-fusion pores and keyholing, cause microstructural heterogeneity and anisotropy. While these features enhance tensile strength due to rapid solidification and fine sub-grains, they create stress concentrators and crack initiation sites that reduce impact toughness. In contrast, the wrought SS 304 microstructure has uniform equiaxed grains and fewer defects, resulting in higher impact toughness compared to AM materials. Notably, a longer impact duration promotes more efficient energy dissipation during an impact event and helps to minimise hazardous effects once the impact ceases. SS 316L ranks as the second-best material in this study for impact-energy absorption, with recorded absorbed energy and impact-duration values exceeding those of AA 6061-T6.

This comparison focuses particularly on specimens produced using metal 3D-printing technology, where both impact and tensile tests demonstrate the capability to approximate the properties of materials manufactured by conventional methods. Moreover, the material's impact response is influenced by its ductility, percentage elongation, and alloying

elements. Ongoing research into metal 3D-printing techniques is essential to ensure that products manufactured in this way can consistently match the performance of conventionally produced materials, while taking advantage of 3D printing's ability to create complex geometries without compromising structural strength.

Future research should include fatigue, high strain-rate and impact tests to confirm long-term performance and assess SS 316L hybrids with lightweight alloys or composites. These advances will boost the commercial potential of 3D-printed SS 316L for energy-absorbing components across automotive, rail, aerospace, marine and industrial sectors, offering strong, lightweight, cost-efficient designs.

Acknowledgement

The authors wish to express their gratitude and thanks to Universiti Teknikal Malaysia Melaka (UTeM) for funding this research under journal scheme.

References

Ali, M. B., Zakaria, K. A., Abdullah, S., & Alkhari, M. R. (2015). Correlation of impact energy from instrumented Charpy impact. *Applied Mechanics and Materials, 815*, 221–226.

ASTM E23-18. (n.d.). *Standard test methods for notched bar impact testing of metallic materials*. ASTM International.

Bunchoo, N., Wongpinkaew, K., Kukiatkulchai, E., Kaewkumsai, S., & Viyanit, E. (2022). Effects of thermal history on sensitization behavior and Charpy impact property of type 316L and 316 stainless steels for applications in a fired heater. *Engineering Failure Analysis, 141*, Article 106654.

Byun, T. S., & Smidts, R. (2004). *Impact tensile testing of stainless steels at various temperatures* (INEEL/EXT-04-01648). Idaho National Laboratory. https://inldigitallibrary.inl.gov/sites/sti/sti/3984786.pdf

Carassus, H., Guérin, J., Morvan, H., Haugou, G., Sadat, T., Guérard, S., & Markiewicz, E. (2022). An experimental investigation into influences of build orientation and specimen thickness on quasi-static and dynamic mechanical responses of selective laser melting 316L stainless steel. *Materials Science and Engineering: A, 832*, Article 142441.

Chen, Y., Zhang, W., Li, X., & Xu, S. (2018). Dynamic impact behaviour and energy absorption characteristics of austenitic stainless steels. *Materials Science and Engineering A, 734*, 254–263.

Chen, Z., Jiang, Z., Wang, F., Zhao, D., Zhang, X., Wang, C., Hao, J., Tong, M., Chen, B., Kong, H. J., Wan, B., Li, R., Liu, G., & Wang, B. (2025). Deformation behavior of additive manufactured 316 L stainless steel using in situ neutron diffraction. *Scientific Reports, 15*, Article 1234.

Coughlin, J. L., Hicks, T., Dougherty, P., & Attanasio, S. (2020). *Development and testing of 316L stainless steel metal additive manufacturing test articles for powder bed fusion and directed energy deposition processes* (Technical Report). Los Alamos National Laboratory.

Duan, X., & Yang, X. (2023). Achieving enhanced strength and ductility in 316L stainless steel via wire arc additive manufacturing using pulsed arc plasma. *Materials Science and Engineering: A, 864*, Article 144497.

Ivañez, I., Moure, M. M., Garcia-Castillo, S. K., & Sanchez-Saez, S. (2015). The oblique impact response of composite sandwich plates. *Composite Structures, 133*, 1127–1136.

Jiang, D., & Ning, F. (2021). Additive manufacturing of 316L stainless steel by a printing-debinding-sintering method: Effects of microstructure on fatigue property. *Journal of Manufacturing Science and Engineering, 143*(2), Article 021003.

Konstantinović, M., Bardel, D., Van Renterghem, W., Van Dyck, S., Badinier, G., Ettaieb, K., Revuelta, A., & Riipinen, T. (2025). Mechanical properties of neutron irradiated 316L stainless steel additively manufactured by laser powder bed fusion: Effect of post-manufacturing heat treatments. *Journal of Nuclear Materials, 582*, Article 154567.

Kumar, S., Singh, J., Kaur, H., & Shahi, A. S. (2024). Cold metal transfer-based wire arc additively manufactured austenitic stainless steel/Inconel 625/superduplex stainless steel wall: Microstructural, corrosion properties, and impact toughness evaluation. *Journal of Materials Engineering and Performance, 33*, 456–470.

Kweon, H. J., Lee, H. M., & Kim, W. S. (2020). Determination of true stress--strain curve of type 304 and 316 stainless steels using a typical tensile test and finite element analysis. *Materials Research Express, 7*(8), Article 086518.

Li, W., Zhao, J., Guo, Z., Xue, X., Zhang, Q., Ma, Z., & Wang, Y. (2023). Study on the mechanical properties and energy absorbing behavior of polyurethane microcellular elastomers (PUME). *Polymers, 15*(3), Article 621.

Lone, S. F., Rathod, D. W., & Ahmad, S. N. (2024). Exploring the feasibility of SS316L fabrication via CMT-based WAAM: A comprehensive study on microstructural, mechanical and tribological properties. *Mechanical Engineering for Society and Industry, 4*(2), 123–135.

Lu, G., & Yu, T. (2003). *Energy absorption of structures and materials*. Woodhead Publishing.

Muhammad Said, N. B., Ali, M. B., & Zakaria, K. A. (2016). Comparison of impact duration between experiment and theory from Charpy impact test. *MATEC Web of Conferences*, Article 01001.

Muhammad Said, N. B., Ali, M. B., & Zakaria, K. A. (2018). Correlation of absorbed energy with PSD energy and area under strain-time graph. *Journal of Advanced Research in Fluid Mechanics and Thermal Sciences, 49*(2), 126–137.

Obeidi, M. A., Uí Mhurchadha, S. M., Raghavendra, R., Conway, A., Souto, C., Tormey, D., Ahad, I., & Brabazon, D. (2021). Comparison of the porosity and mechanical performance of 316L stainless steel manufactured on different laser powder bed fusion metal additive manufacturing machines. *Journal of Materials Research and Technology, 13*, 1234–1245.

Prashanth, K. G., Scudino, S., & Eckert, J. (2019). Impact behaviour of additively manufactured austenitic stainless steels 304 and 316L compared with wrought aluminium alloy 6061-T6. *Materials Science and Engineering A, 746*, 406–417.

Radha, R., & Sreekanth, D. (2015). Mechanical properties of austenitic stainless steel 304L and 316L. *Journal of Bio- and Tribo-Corrosion, 1*(3), Article 24.

Santamaría, R., Salasi, M., Bakhtiari, S., Leadbeater, G., Iannuzzi, M., & Quadir, M. Z. (2022). Microstructure and mechanical behaviour of 316L stainless steel produced using sinter-based extrusion additive manufacturing. *Journal of Materials Science, 57*, 1234–1245.

Shterenlikht, A., Hashemi, S. H., Yates, J. R., Howard, I. C., & Andrews, R. M. (2005). Assessment of an instrumented Charpy impact machine. *International Journal of Fracture, 132*(1), 81–97.

Subramaniyan, M., & Thirugnanasambandam, A. (2024). Wire-arc-additively manufactured bi-metallic structure: Mechanical properties and microstructural characterization. *Proceedings of the Institution of Mechanical Engineers, Part L: Journal of Materials: Design and Applications, 238*(7), 1234–1245.

Tisza, M., & Czinege, I. (2018). Comparative study of the application of steels and aluminium in lightweight production of automotive parts. *International Journal of Lightweight Materials and Manufacture, 1*(4), 229–238. https://doi.org/10.1016/j.ijlmm.2018.09.001

Vora, J., Parmar, H., Chaudhari, R., Khanna, S., Doshi, M., & Patel, V. V. (2022). Experimental investigations on mechanical properties of multi-layered structure fabricated by GMAW-based WAAM of SS316L. *Journal of Materials Research and Technology, 20*, 1234–1245.

Xia, H., Li, W., Zhang, S., & Wang, J. (2022). Influence of strain rate effect on energy absorption characteristics of bio-inspired honeycomb column thin-walled structure under impact loading. *Thin-Walled Structures, 179*, Article 109541.

Xu, M., Guo, H., Wang, Y., Hou, Y., Dong, Z., & Zhang, L. (2023). Mechanical properties and microstructural characteristics of 316L stainless steel fabricated by laser powder bed fusion and binder jetting. *Journal of Materials Research and Technology, 21*, 1234–1245.

Zainuddin, H., Ali, M. B., Zakaria, K. A., Paijan, L. H., Mamat, M. F., & Abu Bakar, M. H. (2024). Investigation of impact properties under instrumented Charpy test. *Journal of Engineering and Technological Sciences, 56*(3), 329–339.

Zhang, M., Paidar, M., Ojo, O., Mehrez, S., Narayanasamy, S., Zain, A., & Mohanavel, V. (2022). Impact of multiple FSP passes on structure, mechanical, tribological and corrosion behaviors of AA6061/316 stainless-steel reinforced Al matrix composites. *Surface and Coatings Technology*, Article 128456.

Zhang, S., Li, X., Li, Y., Chen, X., & Wu, H. (2022). A simulation methodology for analyzing the energy-absorption performance of bio-inspired honeycomb columns under impact loading. *Materials, 15*(20), Article 7224.

Zhang, X., Kenesei, P., Park, J., Almer, J., & Li, M. (2020). In situ high-energy X-ray study of deformation mechanisms in additively manufactured 316L stainless steel. *Journal of Nuclear Materials, 540*, Article 152345.

© 2026 by the authors; licensee Growing Science, Canada. This is an open access article distributed under the terms and conditions of the Creative Commons Attribution (CC-BY) license (http://creativecommons.org/licenses/by/4.0/).